

Multiple magnetic droplet soliton modes


Nahuel Statuto,^{1,2} Christian Hahn,^{3,4} Joan Manel Hernández,² Andrew D. Kent,³ and Ferran Macià^{1,2,*}

¹*Institut de Ciència de Materials de Barcelona (ICMAB-CSIC), Campus UAB, 08193 Bellaterra, Spain*

²*Department of Condensed Matter Physics, University of Barcelona, 08028 Barcelona, Spain*

³*Center for Quantum Phenomena, Department of Physics, New York University, New York, New York 10003, USA*

⁴*Physikalisch-Technische Bundesanstalt, Bundesallee 100, 38116 Braunschweig, Germany*

 (Received 19 December 2018; revised manuscript received 16 February 2019; published 28 May 2019)

Droplet solitons are large amplitude localized spin-wave excitations that can be created in magnetic thin films with uniaxial anisotropy by a spin-polarized current flowing through an electrical nanocontact. Here, we report a low-temperature (4 K) experimental study that shows there are multiple and, under certain conditions, combinations of droplet modes, each mode with a distinct high-frequency spin precession (tens of gigahertz). Low-frequency ($\lesssim 1$ GHz) voltage noise is used to assess the stability of droplet modes. It is found that droplets are stable only in a limited range of applied field and current, typically near the current and field at which they nucleate, in agreement with recent predictions. Applied fields in the film plane favor multiple droplet modes, whereas fields perpendicular to the film plane tend to stabilize a single droplet mode. Micromagnetic simulations are used to show that spatial variation in the energy landscape in the nanocontact region (e.g., spatial variation of magnetic anisotropy or magnetic field) can lead to quantized droplet modes and low-frequency mode modulation, characteristics observed in our experiments.

DOI: [10.1103/PhysRevB.99.174436](https://doi.org/10.1103/PhysRevB.99.174436)

I. INTRODUCTION

Droplet solitons are dynamical magnetic objects that exist in materials with uniaxial anisotropy when the magnetic damping is suppressed [1]. An electrical nanocontact providing spin-polarized current can generate a nonequilibrium magnon population that promotes the creation of droplet solitons [2]. Magnetic droplets are gigahertz nanometer-scale oscillators [3] capable of functioning at zero applied field [4]—thanks to the uniaxial anisotropy—and are tunable with current and magnetic field, which makes them interesting for applications in information processing, including for neuro-morphic computing [5–7].

There has been clear evidence for droplet soliton formation in ferromagnetic materials with perpendicular magnetic anisotropy [8–17], including direct images taken using x-ray microscopy [4,18]. Electrical measurements of voltage across the nanocontact, both ac and dc, provide an understanding of droplet modes due to the giant magnetoresistance effect. Droplet creation produces both a step increase in the dc resistance associated with the partially reversed spins and the appearance of a gigahertz peak in the nanocontact’s noise spectrum associated with the precessing spins. There is an additional low-frequency ($\lesssim 1$ GHz) signal due to droplet motion beneath the nanocontact, which is a signature of droplet instabilities [12,14,19].

An intriguing feature associated with droplet modes reported in experiments is the appearance of multiple small steps in the dc resistance [9,11,12,14] and the existence of different peaks in the noise spectra at high frequency [10,12]

when varying the applied current or the applied magnetic field. If there were multiple droplet modes accessible by varying experimental conditions, it would mean that droplet nano-oscillators could encode more than one oscillation state, each with a certain tunability—a useful feature for coupled oscillators used in pattern recognition [7]. In this paper we report experimental data on multimode droplet solitons including the existence of mode combinations. In order to minimize thermal effects, such as thermally induced mode hopping, we measured nanocontact dc and ac voltage signals at low temperature as a function of applied current and magnetic fields. We found that there is a range of fields and currents where droplet modes are stable—in agreement with predictions made by Wills *et al.* [19].

II. EXPERIMENTAL DETAILS

The experiments were performed on electrical nanocontacts patterned on metallic multilayers consisting of a perpendicularly magnetized free layer (FL) and an easy-plane polarizer layer (PL) (see Fig. 1). The multilayers are composed of permalloy (Py, Ni₈₀Fe₂₀), copper (Cu), nickel (Ni), and cobalt (Co), with the following stack 10Py|10Cu|[0.2Co|0.6Ni] × 6 (numbers in nm) deposited on a 50-nm Cu-bottom electrode on an oxidized Si wafer. Py is the PL and has the magnetization in the film plane; Co|Ni is the FL layer and has perpendicular magnetic anisotropy [20]. The Cu layer magnetically decouples the two layers but allows for an effective spin transport (it is thinner than the spin diffusion length).

We defined electrical contacts of 100–150 nm in diameter to the multilayer stack using e-beam lithography. The resulting device structure is shown in Fig. 1, where the nanocontact is indicated as a nonshaded area on top of the FL. Electrons

*ferran.macia@ub.edu

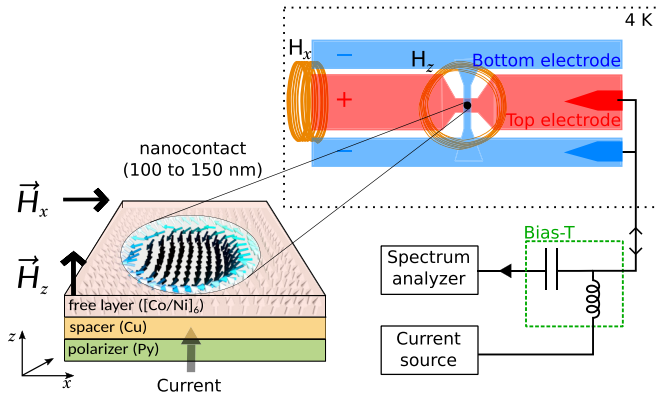


FIG. 1. Schematic of the experimental setup and the magnetic droplet in a multilayer. A current flows through the nanocontact region from the free layer (FL), consisting of 4 nm of a Co/Ni multilayer, to the polarizer layer (PL), made of 10 nm of Py. A positive current is defined by the electron flow from the FL to the PL. The sample is measured in a cryoprobe station at $T = 4$ K, which is equipped with two superconducting magnets: an out-of-plane magnet to apply fields up to 1 T (H_z) and an in-plane magnet to apply fields up to 0.1 T (H_x). A droplet consists of a nearly reversed magnetization region with spins precessing in the x - y plane.

flow from the FL to the PL for positive current polarity ($I > 0$). A magnetic field is applied perpendicular to the film plane to tilt the magnetization of the PL and to control the spin polarization of the applied current. The FL magnetization is illustrated in Fig. 1 by a grid of arrows.

The spin-polarized current carrying angular momentum flows through the FL and creates a torque on the magnetization, eventually producing collective excitations. Variations of the FL magnetization beneath the nanocontact can be measured through variations of the nanocontact magnetoresistance (MR) caused by changes in the relative alignment between PL and FL magnetization [11]. All measurements reported here were done at 4 K in a commercial cryoprobe station, which is equipped with two superconducting magnets capable of applying out-of-plane fields (H_z) and an in-plane fields (H_x).

III. RESULTS

The creation of a droplet produces an increase in dc resistance caused by the partial reversal of magnetization in the nanocontact. There is also a characteristic decrease of the noise frequency associated with droplet formation [2,8,11], which has a different (lower) effective field compared with the uniformly magnetized film. The droplet onset occurs at a spin-polarized current that depends on the applied magnetic field [8–15]. Figure 2 shows measurements of ac and dc resistance for a current sweep at a fixed applied field of 850 mT in the z direction and 50 mT in the x direction. At low currents (< 12.5 mA) no excitations are detected, as seen in Fig. 2(a). Increasing the current value (> 12.5 mA) produces a high-frequency peak at ~ 26 GHz associated with the ferromagnetic resonance (FMR) mode with a quality factor of ~ 590 [Fig. 2(a)]. At a current of 14.9 mA the peak in frequency decreases about 2 GHz and the signal becomes

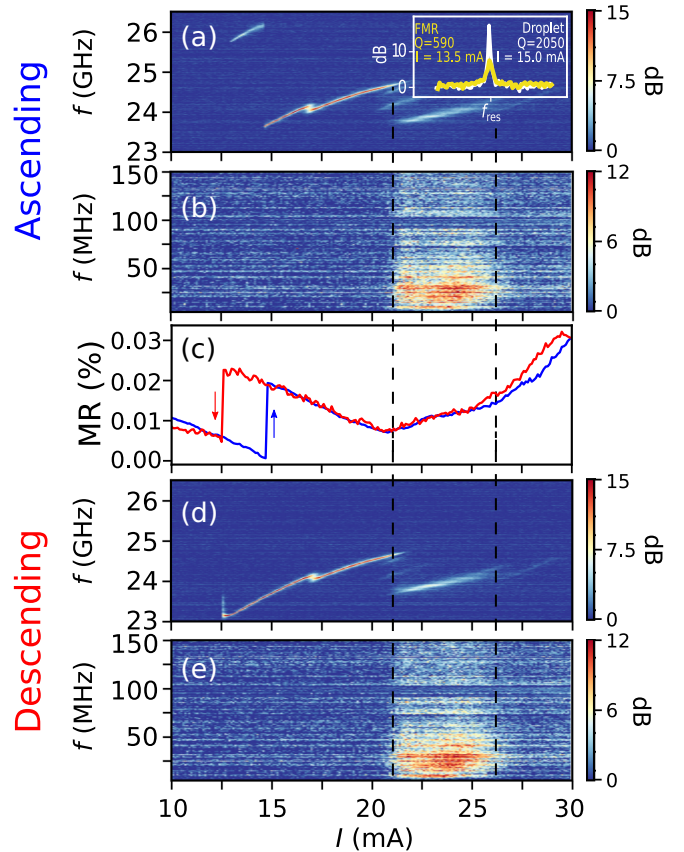


FIG. 2. Both ascending and descending branches of a current sweep. High-frequency [(a) and (d)], low-frequency [(b) and (e)], and dc (c) MR as a function of the applied current at a fixed perpendicular field of 850 mT and an in-plane field applied of 50 mT. In (a), the droplet nucleates at 14.9 mA, where a step in the dc MR is observed (c), blue line, together with a decrease of the peak noise frequency by several gigahertz (a). A further increase of current leads to the appearance of multiple droplet modes accompanied by a low-frequency noise (b) and changes in trend in the dc MR (c). A single parabola is subtracted from the dc MR data. Data on current sweep down can be observed in panels (d) and (e), high and low frequency, respectively. The red line in panel (c) shows the MR for the descending branch showing a small hysteresis that can also be found in panel (d). The inset in panel (a) shows the spectra for the FMR mode at $I = 13.5$ mA, red line with a quality factor of 590, and the droplet mode at $I = 15$ mA, white line with a quality factor of 2050.

higher in amplitude—with a quality factor up to 2050 [see inset in Fig. 2(a)]—and the dc resistance curve presents an abrupt step increase [see Fig. 2(c), blue line]. These signals are signatures of the nucleation of a droplet [8–14].

The movement of a droplet beneath the nanocontact results in variation of the contact resistance and low-frequency noise (voltage oscillations below gigahertz frequencies) that have been linked to drift resonances [12,14,15], which are periodic processes of shifting, annihilation, and creation of droplets. Figure 2(b) plots the low-frequency noise (0–150 MHz) in the same range of currents as in Fig. 2(a). Between 14.9 and 21 mA the droplet is stable, with a powerful high-frequency peak and no associated low-frequency noise. We note that the frequency

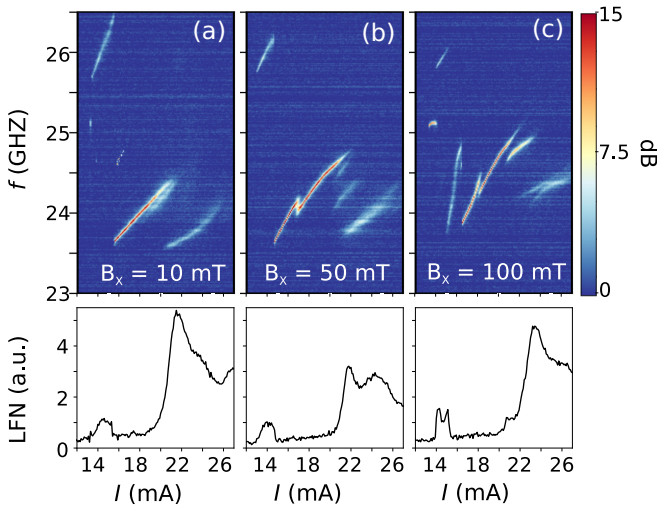


FIG. 3. High-frequency and integrated low-frequency noise (between 10 MHz and 1 GHz) as a function of the applied current at a fixed perpendicular field of 850 mT and at different in-plane fields: (a) 10 mT, (b) 50 mT, and (c) 100 mT. A sharp increase of the integrated low-frequency MR is observed at high currents (above 21 mA) when the main droplet mode splits into multiple modes. The in-plane field also promotes the splitting of the main droplet mode at $I = 16$ mA (b) and $I = 20$ mA (c).

has a step down at around 16 mA, which is completely reproducible and reversible [see also Figs. 2(d) and 2(e) for the descending branches of the current sweep]. For currents higher than 21 mA the situation changes completely and the main high-frequency peak splits into a combination

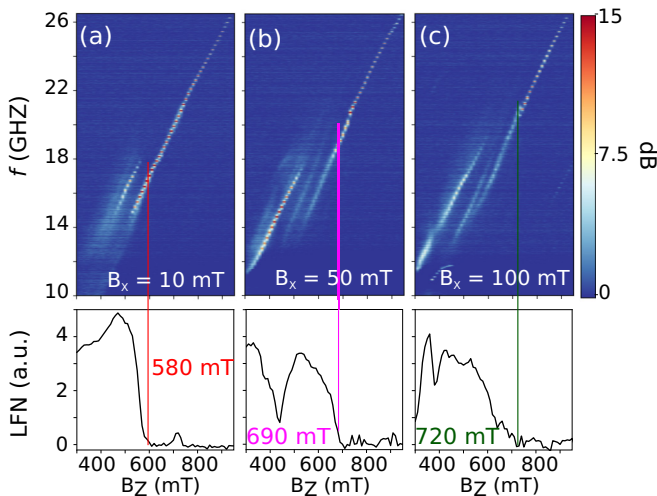


FIG. 4. High-frequency and integrated low-frequency noise (between 10 MHz and 1 GHz) as a function of the applied field at a fixed current of $I = 18$ mA and for different in-plane fields: in (a) 10 mT, in (b) 50 mT, and in (c) 100 mT. Multiple droplet modes are present at low applied fields together with low-frequency noise. At field values higher than 580 mT (a), 690 mT (b), and 720 mT (c) a single peak is observed, with high-quality factors of 2450, 2730, and 1300, respectively, together with the vanishing low-frequency noise, indicate the stability of the droplet mode.

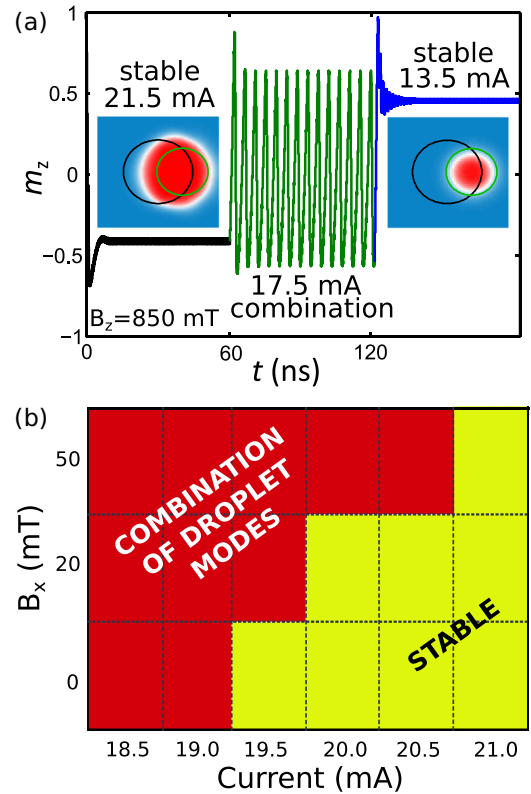


FIG. 5. (a) Evolution of the magnetization, m_z , under a 100-nm-diameter nanocontact for applied currents of $I = 21.5$, 17.5, and 13.5 mA and an applied field perpendicular to the plane of 850 mT. Insets: droplet snapshots correspond to the state at $I = 21.5$ mA and $I = 13.5$ mA. The black circle indicates the position of the nanocontact and the green circle indicates the 2σ for the Gaussian function of 50 mT reducing the overall applied field. (b) State diagram of the droplet state as a function of the applied current and the in-plane field for an out-of-plane field of 850 mT. For a fixed value of the current, the in-plane field can tune the mode of the droplet. For higher values of the in-plane field a combination of droplet modes emerge.

of three weaker peaks with lower frequencies and associated low-frequency noise. Furthermore, the dc MR shows a change in trend, which might be caused partially by an increase in the droplet size: the blue line in Fig. 2(c) shows the dc resistance curve with a parabola subtracted to account for a heating proportional to the square of the applied current. The red curve is for the descending branch. The region with multiple peaks and with low-frequency noise extends from 21 to 26 mA; a quality factor of 320 is measured at $I = 23.2$ mA. Higher current values produce a faint high-frequency signal, an almost invisible low-frequency signal, and another change in the trend of dc resistance.

There is a correlation between ac and dc MR and both measurements show the existence of distinct droplet modes. On the one hand, droplets present a mode with a single and strong high-frequency peak and without low-frequency noise; on the other hand, droplets appear as a combination of high-frequency peaks and a strong low-frequency noise. This behavior of droplet modes as a function of the applied current in Fig. 2 is reproducible and reversible, except for a small

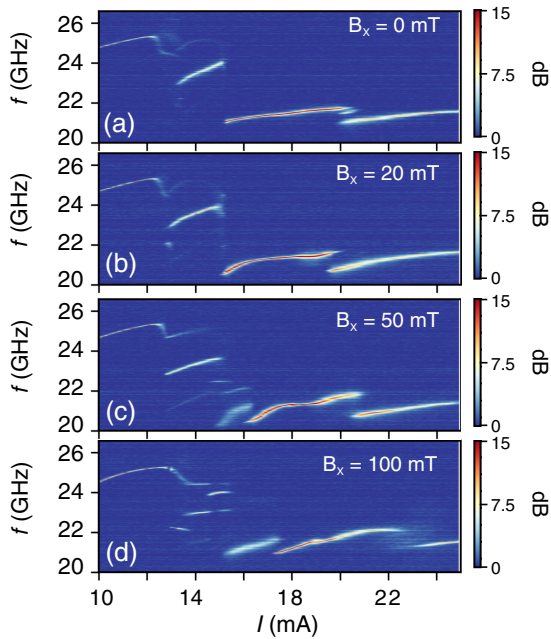


FIG. 6. High-frequency spectra as a function of the current for different in-plane fields and fixed out-of-plane of 750 mT. In-plane fields introduce instabilities while promoting the appearance of a combination of droplet modes

hysteretic response. A current sweep down retraces the steps in both ac and dc MR [see Figs. 2(d) and 2(e), for high- and low-frequency spectra, respectively]. Droplet modes, which appear simultaneously at the same applied field and current, were also observed at different in-plane fields as shown in Appendix A and also in samples from the same batch.

Next, we investigated the control of the observed multiple droplet modes by means of an applied in-plane magnetic field. Oersted fields associated with the electrical current in the nanocontact generate an azimuthally symmetric landscape of

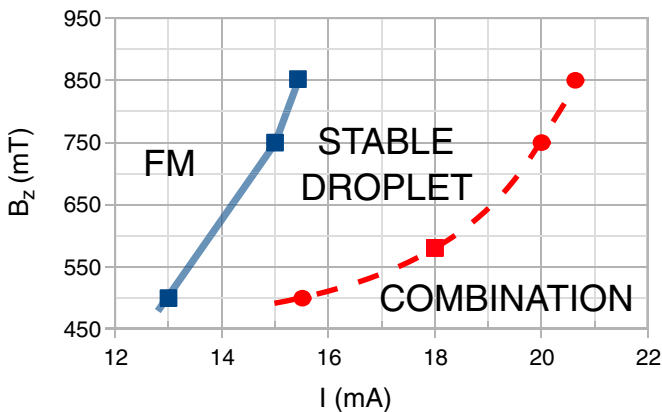


FIG. 7. Phase diagram of the droplet states for the 100-nm-diameter sample at zero in-plane field. For lower current the droplet cannot be excited. Blue squares represent the onset data of the droplet and the blue line is the onset boundary. Red circles represent the boundary between the stable droplet state and the combination of droplet modes obtained from current sweeps for a fixed value of the out-of-plane field. The red square data point is obtained from a field sweep for a fixed value of the current, 18 mA.

in-plane field that can be of the order of 25 mT at the perimeter of the nanocontact (for the currents used in our experiments). There are also in-plane components of the magnetic field caused by material or contact inhomogeneities, which are not azimuthally symmetric and that could produce variations in the droplet localization [21,22]. It is expected [12] that any imbalance of the in-plane field results in a shift of the droplet, causing drift resonances (the droplet shifts outside of the nanocontact where it dissipates, and a new droplet is created beneath the nanocontact). Our experiments show that applying a large enough in-plane field not only produces the appearance of drift instabilities—with associated low-frequency noise—but also favors the generation of multiple droplet modes.

Figure 3 shows the high-frequency and the integrated low-frequency noise (between 10 and 150 MHz) for the same current sweep shown in Fig. 2 under different in-plane fields. The in-plane field splits the single droplet mode into two modes at 17 mA for field values of 50 and 100 mT [Figs. 3(b) and 3(c)] and at 20 mA for a field value of 100 mT [Fig. 3(c)]. However, there is no low-frequency noise associated with the mode changes. At currents above 21 mA the droplet splits again into a different mode (at ~ 23.5 GHz) with associated low-frequency noise; this time the in-plane field also promotes the appearance of additional modes in between the two modes at $I = 21$ mA in Fig. 3(a). The presence of multiple droplet modes is not always associated with low-frequency noise and, conversely, low-frequency noise appears in cases with a single droplet mode. In sum, we found that the effect of in-plane fields when increasing the applied current consists in favoring the splitting of droplet modes with little effect on the modes stability (i.e., no associated low-frequency noise).

In order to understand the correlation between multiple droplet modes and low-frequency noise we studied the effect of variation of an applied field in the z direction at fixed current values—constant current induced Oersted fields. Figure 4 shows high-frequency spectra, and integrated low-frequency spectra, for perpendicular magnetic field sweeps at a constant applied current of 18 mA and for different applied in-plane fields. At a current of 18 mA droplet modes form at a low applied field (< 300 mT). By increasing the applied field the peak noise frequency increases as well with a slope of ~ 28 GHz/T, which corresponds to the gyromagnetic ratio, $\gamma/2\pi$. The droplet mode at low fields has associated low-frequency noise indicating a low stability. A further increase of the applied field produces a variation of droplet modes with a split into different modes—including a range of fields showing a combination of droplet modes. There is an applied field where the low-frequency noise vanishes corresponding to the existence of a single and higher amplitude peak in the high-frequency spectra. We marked those field values with colored lines in Fig. 4. Quality factors of 2450, 2730, and 1300 are obtained right after the marked field values. Our data indicates that higher fields tend to stabilize droplet modes. The presence of in-plane fields shifts the stabilizing values toward higher fields. These results are in agreement with Wills *et al.* [19] that predicted that droplet modes would be stable only close to its boundaries of nucleation, which means either at low currents for a given field or at large fields at a fixed current.

We have created a toy model to show that a nonuniform energy landscape of the internal applied field of the FL

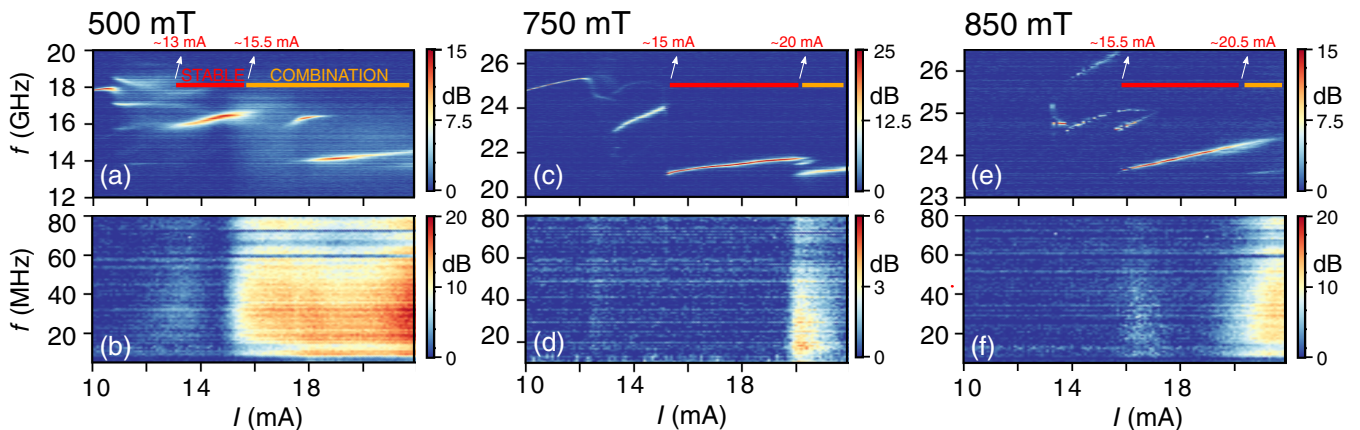


FIG. 8. Ascending branches of a current sweep for three different out-of-plane fields, 500, 750, and 850 mT, at zero in-plane field. High-frequency [(a), (c), and (e)] and low-frequency [(b), (d) and (f)] noise as a function of the applied current. Red horizontal lines represent the stable droplet region and the orange line represents the combination of droplet mode region. This data was used to create Fig. 7.

can result in the appearance of discrete droplet modes with slightly different precession frequencies and dimensions. Using micromagnetic simulations we defined an artificial energy landscape for the applied field consisting of a uniform field perpendicular to the film plane of 850 mT, as in experiment, plus a small region of about 35 nm where the applied field decreases smoothly down to 780 mT (see the Supplemental Material for the code and details [23]).

An applied current of 21.5 mA first localizes the droplet mostly beneath the nanocontact with a small shift toward the region where the applied field is smaller. The precession frequency is 24.49 GHz. A much smaller current of 13.5 mA still maintains the droplet mode but now the droplet lies precisely at the region with a smaller field [21,22]. The precession frequency is now 25.21 GHz. An intermediate applied current of 17.5 mA produces a combination of the two mentioned modes with an oscillating frequency of ~ 230 MHz. Figure 5(a) shows the magnetization in the perpendicular direction within the nanocontact region for a current sweep having values of $I = 13.5, 17.5,$ and 21.5 mA. Snapshots of the droplet are plotted as insets showing the two different modes.

Next, we add an in-plane field to the same simulation routine; we sweep down the applied current from a large value of 21.5 mA and record the moment when the combination of droplet modes appear. Figure 5(b) shows a phase diagram of the droplet state as a function of the in-plane field and the applied current at a fixed value of the out-of-plane field of 850 mT. At high currents the droplet is stable occupying the full nanocontact (yellow region). When the current decreases a combination of droplet modes appears, as seen in Fig. 5(a), and its appearance depends on the applied in-plane field: a larger in-plane field requires a larger current for stabilization.

Our experiments have been done at low temperature to minimize the thermal effects that might cause mode hopping. Although the nanocontact temperature could be much higher than the bath temperature [24], our results indicate that the existence of combinations of droplet modes is not driven mainly by thermal energies. The micromagnetic modeling illustrates the possibility of having different droplet modes given by the energy landscape. In the example presented in Fig. 5 we

observe that the mode that is preferred depends on the applied current—which changes both the spin-transfer torque and the Oersted fields associated with the charge current. The FL is polycrystalline with a grain size of the order of tens of nanometers and variations of the FL magnetic anisotropy can exist on this scale, which could explain the modulation of the magnetic energy in the FL. The results would also explain both the variations of observed droplet modes in different nanocontacts and the reproducibility of measurements with a combination of droplet modes within the same nanocontact.

IV. CONCLUSIONS

We have studied multiple droplet modes—including a combination of droplet modes—in a spin nanocontact. We have observed the existence of different and quantized droplet modes that are accessed by varying applied fields and currents. We found that droplet modes at low currents have a larger high-frequency amplitude and a better quality factor with no associated low-frequency noise, independent of the number of droplet modes. When droplet modes destabilize—at large currents or at low fields—there is an associated low-frequency noise, which is even larger when there is an existence of a combination of droplet modes. Our study shows that spin torque nano-oscillators based on droplet solitons have many different accessible modes in addition to their nonlinearity and stochasticity, which could be exploited in neuromorphic [5–7] or reservoir computing [25,26].

ACKNOWLEDGMENTS

F.M. acknowledges support from the RyC through Grant No. RYC-2014-16515 and from MINECO through the SO Program (Grants No. SEV-2015-0496 and No. MAT2017-85232-R). J.M.H., N.S., and F.M. acknowledge funding from MINECO through Grant No. MAT2015-69144-P. N.S. acknowledges funding from SURDEC through the research training grant FI-DGR. A.D.K. acknowledges support from the National Science Foundation under Grant No. DMR-1610416. Research at NYU related to neuromorphic computing was supported as part of the

Quantum-Materials for Energy Efficient Neuromorphic-Computing, an Energy Frontier Research Center funded by the U.S. Department of Energy (DOE), Office of Science, Basic Energy Sciences (BES), under Award DE-SC0019273.

APPENDIX A: EFFECT OF IN-PLANE FIELDS

High-frequency data as a function of the applied current at 750 mT out-of-plane field is provided for different in-plane fields in Fig. 6. For currents lower than 15 mA a FMR-like signal is observed at about 24 GHz. Then, at 15 mA, a 3-GHz step decrease in the peak noise frequency indicates the droplet nucleation and the high-frequency peak becomes larger. The droplet remains stable until 20 mA where another step decrease is observed accompanied by a step-like increase of the low-frequency noise and a decrease of the high-frequency signal power, as can be observed in Fig. 8(d).

The effect of the in-plane field can be observed in panels (b) 20 mT, (c) 50 mT, and (d) 100 mT. The in-plane field promotes the appearance of a combination of droplet modes just after the nucleation of the droplet, shifting the stable droplet mode toward higher applied currents

(from 15 mA without in-plane field to 17.5 mA for a 100 mT of in-plane field).

APPENDIX B: PHASE DIAGRAM OF DROPLET MODES

Combining the high- and low-frequency data from both current and field sweeps, we plot a phase diagram of the droplet states. Figure 7 shows the state of the droplet as a function of the applied current and the out-of-plane magnetic field at zero in-plane field. Blue squares represent the onset data for the droplet from current sweeps—and the blue line is the onset boundary. Inside the droplet region we can distinguish between a stable droplet and a combination of droplet mode regions, marked as red circles (experimental points where the multiple modes with low-frequency noise appear). An additional red square is added from measurements from a field sweep for a fixed value of the current, 18 mA, where the combination of droplet modes disappear.

Figure 8 shows the high- and low-frequency noise spectra for applied fields of 500, 750, and 850 mT out of the film plane at zero in-plane field. Data corresponds to the points used to create the diagram of Fig. 7.

-
- [1] A. M. Kosevich, B. A. Ivanov, and A. S. Kovalev, *Phys. Rep.* **194**, 117 (1990).
- [2] M. A. Hofer, T. J. Silva, and M. W. Keller, *Phys. Rev. B* **82**, 054432 (2010).
- [3] T. Chen, R. K. Dumas, A. Eklund, P. K. Muduli, A. Houshang, A. A. Awad, P. Dürrenfeld, B. G. Malm, A. Rusu, and J. Åkerman, *Proc. IEEE* **104**, 1919 (2016).
- [4] S. Chung, Q. T. Le, M. Ahlberg, A. A. Awad, M. Weigand, I. Bykova, R. Khymyn, M. Dvornik, H. Mazraati, A. Houshang, S. Jiang, T. N. Anh Nguyen, E. Goering, G. Schütz, J. Gräfe, and J. Åkerman, *Phys. Rev. Lett.* **120**, 217204 (2018).
- [5] N. Locatelli, V. Cros, and J. Grollier, *Nat. Mater.* **13**, 11 (2014).
- [6] J. Torrejon, M. Riou, F. A. Araujo, S. Tsunegi, G. Khalsa, D. Querlioz, P. Bortolotti, V. Cros, K. Yakushiji, A. Fukushima, H. Kubota, S. Yuasa, M. D. Stiles, and J. Grollier, *Nature (London)* **547**, 428 (2017).
- [7] M. Romera, P. Talatchian, S. Tsunegi, F. A. Araujo, V. Cros, P. Bortolotti, J. Trastoy, K. Yakushiji, A. Fukushima, H. Kubota, S. Yuasa, M. Ernoult, D. Vodenicarevic, T. Hirtzlin, N. Locatelli, D. Querlioz, and J. Grollier, *Nature (London)* **563**, 230 (2018).
- [8] S. M. Mohseni, S. R. Sani, J. Persson, T. N. A. Nguyen, S. Chung, Y. Pogoryelov, P. K. Muduli, E. Iacocca, A. Eklund, R. K. Dumas, S. Bonetti, A. Deac, M. A. Hofer, and J. Åkerman, *Science* **339**, 1295 (2013).
- [9] S. Chung, S. M. Mohseni, S. R. Sani, E. Iacocca, R. K. Dumas, T. N. Anh Nguyen, Y. Pogoryelov, P. K. Muduli, A. Eklund, M. Hofer, and J. Åkerman, *J. Appl. Phys.* **115**, 172612 (2014).
- [10] S. M. Mohseni, S. R. Sani, R. K. Dumas, J. Persson, T. N. Anh Nguyen, S. Chung, Y. Pogoryelov, P. K. Muduli, E. Iacocca, A. Eklund, and J. Åkerman, *Physica B* **435**, 84 (2014).
- [11] F. Macià, D. Backes, and A. D. Kent, *Nat. Nanotechnol.* **9**, 992 (2014).
- [12] S. Lendínez, N. Statuto, D. Backes, A. D. Kent, and F. Macià, *Phys. Rev. B* **92**, 174426 (2015).
- [13] S. Chung, S. M. Mohseni, A. Eklund, P. Dürrenfeld, M. Ranjbar, S. R. Sani, T. N. Anh Nguyen, R. K. Dumas, and J. Åkerman, *Low Temp. Phys.* **41**, 833 (2015).
- [14] S. Chung, A. Eklund, E. Iacocca, S. M. Mohseni, S. R. Sani, L. Bookman, M. A. Hofer, R. K. Dumas, and J. Åkerman, *Nat. Commun.* **7**, 11209 (2016).
- [15] S. Lendínez, J. Hang, S. Vélez, J. M. Hernández, D. Backes, A. D. Kent, and F. Macià, *Phys. Rev. Appl.* **7**, 054027 (2017).
- [16] J. Hang, C. Hahn, N. Statuto, F. Macià, and A. D. Kent, *Sci. Rep.* **8**, 6847 (2018).
- [17] B. Divinskiy, S. Urazhdin, V. E. Demidov, A. Kozhanov, A. P. Nosov, A. B. Rinkevich, and S. O. Demokritov, *Phys. Rev. B* **96**, 224419 (2017).
- [18] D. Backes, F. Macià, S. Bonetti, R. Kukreja, H. Ohldag, and A. D. Kent, *Phys. Rev. Lett.* **115**, 127205 (2015).
- [19] P. Wills, E. Iacocca, and M. A. Hofer, *Phys. Rev. B* **93**, 144408 (2016).
- [20] F. Macià, P. Warnicke, D. Bedau, M.-Y. Im, P. Fischer, D. Arena, and A. D. Kent, *J. Magn. Magn. Mater.* **324**, 3629 (2012).
- [21] V. E. Demidov, S. Urazhdin, and S. O. Demokritov, *Nat. Mater.* **9**, 984 (2010).
- [22] S. Bonetti, R. Kukreja, Z. Chen, F. Macià, J. M. Hernández, A. Eklund, D. Backes, J. Frisch, J. Katine, G. Malm, S. Urazhdin,

- A. D. Kent, J. Stöhr, H. Ohldag, and H. A. Dürr, *Nat. Commun.* **6**, 8889 (2015).
- [23] See Supplemental Material at <http://link.aps.org/supplemental/10.1103/PhysRevB.99.174436> for micromagnetic code and details.
- [24] S. Petit-Watelot, R. M. Otxoa, M. Manfrini, W. Van Roy, L. Lagae, J.-V. Kim, and T. Devolder, *Phys. Rev. Lett.* **109**, 267205 (2012).
- [25] D. Pinna, F. Abreu Araujo, J.-V. Kim, V. Cros, D. Querlioz, P. Bessiere, J. Droulez, and J. Grollier, *Phys. Rev. Appl.* **9**, 064018 (2018).
- [26] D. Marković, N. Leroux, M. Riou, F. Abreu Araujo, J. Torrejon, D. Querlioz, A. Fukushima, S. Yuasa, J. Trastoy, P. Bortolotti, and J. Grollier, *Appl. Phys. Lett.* **114**, 012409 (2019).